



Magnetic and optical investigations on LaFeO₃ powders with different particle sizes and corresponding ceramics

Roberto Köferstein, Lothar Jäger, Stefan G Ebbinghaus

► To cite this version:

Roberto Köferstein, Lothar Jäger, Stefan G Ebbinghaus. Magnetic and optical investigations on LaFeO₃ powders with different particle sizes and corresponding ceramics. Solid State Ionics, 2013, 249-250, pp.1-5. 10.1016/j.ssi.2013.07.001 . hal-01995704

HAL Id: hal-01995704

<https://hal.science/hal-01995704>

Submitted on 27 Jan 2019

HAL is a multi-disciplinary open access archive for the deposit and dissemination of scientific research documents, whether they are published or not. The documents may come from teaching and research institutions in France or abroad, or from public or private research centers.

L'archive ouverte pluridisciplinaire **HAL**, est destinée au dépôt et à la diffusion de documents scientifiques de niveau recherche, publiés ou non, émanant des établissements d'enseignement et de recherche français ou étrangers, des laboratoires publics ou privés.

Solid State Ionics 249–250 (2013) 1–5

(doi: 10.1016/j.ssi.2013.07.001)

<http://dx.doi.org/10.1016/j.ssi.2013.07.001>

**Magnetic and optical investigations on LaFeO₃ powders with
different particle sizes and corresponding ceramics**

Roberto Köferstein^{*}, Lothar Jäger, Stefan G. Ebbinghaus

*Institute of Chemistry, Inorganic Chemistry, Martin-Luther-University Halle-Wittenberg,
Kurt-Mothes-Strasse 2, 06120 Halle, Germany.*

^{*} Corresponding author. Tel.: +49-345-5525630; Fax: +49-345-5527028.
E-mail address: roberto.koefenstein@chemie.uni-halle.de

Abstract. The optical and magnetic properties of nano-LaFeO₃ powders prepared by a starch assisted soft-chemistry synthesis and corresponding ceramics have been investigated. Magnetic measurements on LaFeO₃ powders with crystallite sizes of 37–166 nm show pronounced magnetization hysteresis loops. Measurements at 300 K reveal that the coercivity (H_c) of 19–32 kOe depends on the crystallite size, whereas the low remanence values (M_r) of roughly 0.2 emu/g and the maximal magnetization (M_{max}) at 90 kOe of 1.05–0.85 emu/g are only slightly changing. Investigations at 10 K reveal a loop shift (exchange bias) up to 12 kOe in the negative direction depending on the crystallite size. Ceramic bodies, sintered at ≥ 1300 °C possess a considerably reduced hysteresis loop. H_c is decreased up to 3.0 kOe, whereas M_r

and M_{\max} are slightly increasing. None of the samples reaches saturation at 90 kOe indicating an anti-ferromagnetic ordering of the spins. The optical band gaps of the LaFeO_3 samples were determined by means of diffuse reflectance spectra. For all LaFeO_3 powders similar band gaps of 2.65 eV were observed. However, ceramics with grain-size significantly larger than 250 nm show smaller band gap values up to 2.12 eV.

Keywords: lanthanum orthoferrite; perovskite; ceramic; nano-particles, optical band gap; magnetic properties

1. Introduction

Perovskite materials based on lanthanum orthoferrite (LaFeO_3) are of great importance because of their broad application potential in advanced technologies. Substituted LaFeO_3 compounds have been studied as membrane-reactor material for the partial oxidation of methane to syngas [1,2]. LaFeO_3 based materials reveal catalytic potential for the decomposition of e.g. hydrocarbons, chlorinated Volatile Organic Compounds (VOCs) or in the reaction between NO and CO [3,4,5,6]. They are also promising candidates as catalysts in heterogeneous Fenton-like reactions to generate $\cdot\text{OH}$ radicals from H_2O_2 [7,8]. Due to the small band gap LaFeO_3 can be used in photocatalytic applications [9,10,11]. Furthermore, lanthanum orthoferrites are also applied as sensor materials [12,13,14] and as electrode material in Solid Oxide Fuel Cells (SOFCs) [15,16,17,18].

LaFeO_3 is a canted G-type anti-ferromagnet with a Néel temperature of 467 °C [19]. At room temperature it crystallizes in an orthorhombically distorted perovskite lattice.

To obtain fine-grained/nano-sized LaFeO_3 powders several wet-chemical syntheses have been developed such as precursor methods [20,21,22,23] sol-gel and combustion routes [9,24,25, 26] or by a microemulsion route [5,27].

Optical band gap (E_g) values between about 2.1 and 3.85 eV have been reported for LaFeO_3 [9,10,25,28,29,30,31]. The optical band gap depends on preparation method and particle size [32,33]. On the other hand, the band gaps of LaFeO_3 were determined by different techniques, what might be one of the reasons for deviating values. Calculations based on the local spin density approximation (LSDA) by *Shein* et al. [34] and *Yang* et al. [35] resulted in band gaps of 2.52 eV and 2.1 eV, respectively.

The aim of this paper is to investigate the magnetic and optical properties of nano-sized LaFeO_3 prepared by a simple and fast preparation route using starch as a complexation agent as reported in a previous paper [36]. Additionally, coarse-grained LaFeO_3 ceramic bodies obtained by an additional sintering step were studied. The optical band gap and the field-dependent magnetization were measured with respect to the particle size as well as to the calcination-/sintering conditions.

2. Experimental

2.1. Material preparation

LaFeO_3 samples were prepared by a decomposition process using starch both as complexation agent and gellant as described elsewhere [36]. Briefly, $\text{La}(\text{NO}_3)_3 \cdot 6\text{H}_2\text{O}$ (0.006 mol, *Merck*) and $\text{Fe}(\text{NO}_3)_3 \cdot 9\text{H}_2\text{O}$ (0.006 mol, *Merck*) were dissolved in 15 ml water and 2 g soluble starch (*Sigma-Aldrich*) was added. The resulting suspension was continuously stirred on a heating plate at room temperature for 15 min. Afterwards the temperature was raised to about 120 °C and the mixture was stirred until it turned to a highly viscous orange gel.

The obtained (LaFe)-gel was calcined in static air up to 1000 °C (heating-/cooling rate 5 K/min) as summarized in Tab. 1 (powders **1a–1e**). The LaFeO_3 powder **1a** calcined at 570 °C for 2 h was used to produce ceramic bodies (**S1–S6**). For that purpose powder **1a** was mixed with 5 mass% of a saturated aqueous polyvinyl alcohol (PVA) solution as a pressing aid,

pressed into pellets and sintered between 1200 and 1450 °C for 1 and 10 h with a heating-/cooling rate of 5 K/min in static air [36].

Chemical analyses (gravimetry, complexometry [37,38]) of the samples indicated a La/Fe ratio of 0.998.

2.2. Characterization

The specific surface area was determined using nitrogen three-point BET (Nova 1000, *Quantachrome Corporation*). The equivalent BET particle diameters were calculated assuming a spherical or cubic particle shape [39]. Diffuse reflectance spectra were obtained at room temperature in the range 380–1000 nm using a *Perkin Elmer* UV–VIS spectrometer Lambda 19. BaSO₄ was used as a white standard. Magnetic measurements were carried out using a *Quantum Design* PPMS 9. The magnetizations were measured at 300 K and 10 K with magnetic field cycling between –90 and +90 kOe.

3. Results and discussion

3.1. Samples characterization

In a previous paper [36] we have already reported on the temperature-dependent phase evolution of LaFeO₃ nano-scaled powders and their sintering behaviour resulting in ceramic bodies. In this contribution we describe the magnetic and optical properties of these samples. Table 1 summarized the calcination conditions, the specific surface areas, and the particle-/crystallite sizes of these powders. At the lowest calcination temperature of 570 °C powder **1a** possesses a BET surface area of 25.7 m²/g and a crystallite size of 37 nm. TEM images revealed an agglomerated powder with porous features. The individual particles are mainly in the range of about 20 to 60 nm. Up to 1000 °C (powder **1e**) the BET surface area decreases to 6.5 m²/g and the crystallite size increases to 166 nm. Ceramic bodies were obtained by pressing powder **1a** to compacts followed by sintering between 1200 and 1600 °C for 1 and

10 h in air. Sintering conditions, relative densities and the grain size ranges are also listed in Tab. 1.

3.1. Magnetic measurements

Fig. 1 exemplarily shows the magnetization (M) depending on the applied magnetic field (H) at 300 K for the LaFeO_3 powders **1a**, **1b**, and **1e**. The samples **1a–1e** show hysteresis loops at 300 K with low remanences (M_r) of about 0.2 emu/g and large coercivities (H_c) up to 32 kOe. We found that the coercivity depends on the calcination temperature and thus on the crystallite size and reaches a maximum at a crystallite size of 106 nm (900 °C). Further calcination at 1000 °C (crystallite size 166 nm) results in a slight reduced coercivity as depicted in Fig. 2. The remanence varies only slightly with the crystallite size and the magnetization at 90 kOe (M_{max}) decreases with raising crystallite size (Tab. 2). Obviously, no saturation is reached but the magnetization increases almost linearly with H .

Magnetic measurements at 300 K on the ceramic bodies made from powder **1a** show that the area of the hysteresis loop is strongly reduced for sintering temperatures ≥ 1300 °C (Fig. 3, Tab. 2). M_{max} and M_r first increase with raising sintering temperature but above 1300 °C they change only slightly. It can be seen from Table 2 that the sintering time has only a marginal influence on M_{max} and M_r , respectively. In contrast, the coercivity decreases both with increasing sintering temperature and sintering time.

The magnetic behaviours of the ceramic bodies at 10 K are similar to the ones at 300 K. The values of M_r , H_c , and M_{max} are only slightly higher by trend (Tab. 2). In contrast, in magnetic measurements of the LaFeO_3 powders (**1a–1e**) at 10 K we found different coercivity values for decreasing and increasing fields as demonstrated for powder **1d** in Fig. 4a. This exchange bias-like behaviour results in a significant shift of the M – H loops (ΔH_c) in the negative direction with respect to the origin ($H = 0$). In consideration of the studies of *Nogues* and *Schuller* [40] and *Leslie-Pelecky* and *Schalek* [41] the coercivity shift is defined as $\Delta H_c =$

$|0.5(H_{c(df)} + H_{c(if)})|$, where $H_{c(df)}$ is the coercivity at decreasing field and $H_{c(if)}$ is the coercivity at increasing field, i.e. powder **1a** has coercivity values of -14.4 kOe ($H_{c(df)}$) and $+0.48$ kOe ($H_{c(if)}$) resulting in $\Delta H_c = 7.0$ kOe. ΔH_c was found to depend on the crystallite size. For very small sizes between about 40 and 60 nm ΔH_c increases to a maximum of 12.3 kOe while for larger crystallite sizes ΔH_c decreases (Fig. 4b). An analogous behaviour was also found for nano-sized NiO particles, BiFeO₃, Bi₂Fe₄O₉ and for nano YFeO₃ [42,43,44,45]. Wang and Gong [46] reported on a small loop shift for LaFeO₃ nano-spheres, and loop shifts up to 1.5 kOe were observed in nano-LaFeO₃ prepared by a sol-gel route [47]. As a result of the exchange-bias like shift and the resulting asymmetry of the hysteresis curve the values of the maximum magnetization at $H = +90$ kOe and -90 kOe are different. For powder **1a** M_{max} is 1.36 emu/g for $H = +90$ kOe while at $H = -90$ kOe M_{max} accounts to only 1.08 emu/g. The difference in the maximal magnetizations (ΔM_{max}) at $H = +90/-90$ kOe decreases with raising particle size similar to the development of ΔH_c (Fig. 4b). Additionally we observed that ΔH_c depends on the number (n) of field cycles. ΔH_c decreases with the number of consecutive hysteresis loops as demonstrated for powders **1a** and **1e** in the inset in Fig. 4b. This so-called *training effect* is often observed in ferromagnetic/antiferromagnetic thin films [40,48,49] and also in e.g. NiFe₂O₄/NiO nano-composites [50] and core-shell Fe/Fe₃O₄ nano-particles [51]. Manna et al. [52] and Passamani et al. [53] found the *training effect* in Mn-doped BiFeO₃ nano-particles and in ball-milled NiFe₂O₄ nano-particles, respectively. In general, loop shifts occur in materials with ferromagnetic/anti-ferromagnetic interfaces (exchange bias) [40,54]. Ahmadvand et al. [47] discuss an exchange coupling between a ferromagnetic-like shell and an antiferromagnetic core in nano-LaFeO₃ particles. From the results above the loop shift is a finite size effect. Nanoparticles exhibit a large disordered surface with reduced coordination of surface spins. Calculations by Kodama et al. [42] on NiO nanoparticles showed that the loop shift originates from the interaction between the reduced coordinated surface spins and

the core. Therefore, we did not observe any shift of the hysteresis loops for LaFeO₃ ceramic bodies because of their large grain sizes.

The magnetization curves of all samples both at 300 K and 10 K clearly show that up to 90 kOe the saturation magnetization is not yet reached, indicating mainly an anti-ferromagnetic ordering of the spins [30,55]. Additionally, the shape of the hysteresis loops is characteristic for a canted anti-ferromagnet in which due to the canting an uncompensated moment remains leading to a weak ferromagnetic characteristic [19,56,57]. That behaviour is also observed in other LaFeO₃ samples as well as in Bi- and Y-orthoferrites [43,47,58].

3.3. Diffuse reflectance measurements

Fig. 5 shows the diffuse reflectance spectra of selected LaFeO₃ powders **1a**, **1c**, and **1e** showing strong visible-light absorption. The *Kubelka–Munk* theory was used for analysis of the diffuse reflectance spectra. It combines the reflectance data with the absorption coefficient as shown in equation 1 [59,60]:

$$F(R) = \frac{\alpha}{s} = \frac{(1 - R)^2}{2R} \quad (1)$$

where $F(R)$ is the *Kubelka–Munk* function, R the reflectance, α the absorption coefficient and s is the scattering factor. Since the scattering factor is wavelength independent, $F(R)$ is proportional α [60].

There are various techniques to extract the band gap energy from diffuse reflectance measurements [61]. A simple way to determine the optical band gap is plotting of e.g. the reflectance or absorbance versus wavelength. The onset of the linear increase in diffuse reflectance/ absorbance is taken as the energy of the band gap. As pointed out by *Lopez* and

Gomez [62] and *Nowak et al.* [61] the band gap energy slightly depends on the graphic representation and the above mentioned technique does not lead to an accurate band gap energy. The optical band gap for LaFeO_3 from diffuse reflectance spectra vary from 2.1 to 3.85 eV [9,10,25,28,29,30,31,63]. Apart from different LaFeO_3 samples with different particle sizes and synthesis routes the reason for these discrepancies also lie in the different graphical determination techniques. To accurately determine the band gap it is necessary to find the type of transition [61,64]. The *McLean* analysis [65,66] of the absorption edge was applied to find the type of transition and to determine the optical band gap by equation 2 [67].

$$\alpha h\nu = k(h\nu - E_g)^{1/n} \quad (2)$$

where k is an energy-independent constant, E_g the optical band gap. The exponent n is determined by the type of transition: $n = 2$ for direct allowed transitions, $n = 2/3$ for direct forbidden transitions, $n = 1/2$ for indirect allowed transitions and $n = 1/3$ for indirect forbidden transitions. Since $F(R)$ is proportional to α (see above) the exponent n can be determined by plotting $(F(R) \cdot h\nu)^n$ vs. $h\nu$. The best fit to a straight line near the absorption edge was found for $n = 2$ indicating a direct allow transition. Consequently, equation 2 can be transformed to:

$$F(R) \cdot h\nu = k(h\nu - E_g)^{1/2} \quad (3)$$

From a plot of $(F(R) \cdot h\nu)^2$ vs. $h\nu$ (inset in Fig. 5) the band gap energy can be determined by extrapolating the slope to $F(R) \rightarrow 0$.

The band gap energy for powder **1a** with a crystallite size of 37 nm was determined as 2.65(2) eV. The value of the band gap does not change significantly up to a calcination temperature of

1000 °C corresponding to a crystallite size of 166 nm (Tab. 3). An analogous result was also found for LaFeO₃ powders prepared from a sol-gel synthesis [9].

Ceramic bodies made from powder **1a** show reduced band gaps (Tab. 3). Sintering at 1200 °C for 1 h results in ceramic bodies (**S1-1**) with grain sizes of 0.25 to 0.9 nm and the band gap was found to be 2.51(4) eV. Raising the sintering temperature to 1300 °C results in grains between 0.6–2.5µm (**S3-1**) and the optical band gap is downshifted to 2.13(1) eV. Higher sintering temperatures and thus larger grain sizes do not lead to a significant change of the band gap. Additionally, sintering with prolonged soaking time up to 10 h has no significant effect on the band gap energy.

As shown the LaFeO₃ powders with crystallites sizes between 37 and 166 nm has higher band gap energies than the coarse-grained ceramic bodies with grain sizes considerably larger than 250 nm. It is a well-know effect that small particles tend to exhibit increased band gaps [32,33]. This effect allows to influences the colour and photocatalytic activities of the samples during the transition from micro to nano particles.

Conclusion

We investigated the magnetic and optical properties of nano-sized LaFeO₃ powders prepared by decomposition of a starch-based (LaFe)-gel and ceramic bodies prepared from these powders. Calcination in air of the (LaFe)-gel from 570 to 1000 °C yield very fluffy phase-pure LaFeO₃ powders with crystallite sizes between 37 and 166 nm. The powders show pronounced M–H hysteresis loops. At 300 K the coercivity depends on the crystallite size and for particles with sizes of about 120 nm reaches maximum values of up to 32 kOe. In contrast very similar remanences around 0.2 emu/g, magnetization between 0.85 and 1.05 emu/g at 90 kOe were obtained for all powders at 300 K. Magnetization measurements at 10 K revealed that the LaFeO₃ powders show an exchange-bias like shift (ΔH_c) of the hysteresis loops. A

maximum shift of 12 kOe was observed for a crystallite size of about 50 nm. The ceramic bodies show a drastic decrease of both remanence and coercivity values with increasing grain sizes, leading to H_c values down to 3 kOe. The M–H hysteresis loops show that no saturation up to a magnetic field of 90 kOe was reached for any of the samples, suggesting an anti-ferromagnetic ordering of the spins. The optical band gaps were determined by means of diffuse reflectance spectra. Almost identical band gaps of 2.65 eV were determined for all powder samples. In contrast, ceramic bodies (grain sizes larger than 250 nm) show smaller band gaps between 2.51 and 2.12 eV, depending on the grain sizes.

Acknowledgements

Financial support by the German Science Foundation within the Collaborative Research Centre (SFB 762) “Functionality of Oxide Interfaces” is gratefully acknowledged.

Table 1

Heat treatment, BET surface area and particle-/grain sizes of LaFeO₃ powders and ceramic bodies

Powder	Calcination procedure	S _{BET} (m ² /g)	d _{BET} (nm) ¹⁾	d _{cryst} (nm) ²⁾
1a	570 °C/ 2h	25.7	35	37
1b	700 °C/ 2h	17.1	53	54
1c	800 °C/ 2h	12.0	75	80
1d	900 °C/ 2h	9.1	99	106
1e	1000 °C/ 2h	6.5	139	166
Ceramics ³⁾	Sintering procedure	Relative density (%)	Grain-size range (μm) ⁴⁾	
S1-1	1200 °C/ 1h	50	0.25–0.9	
S2-1	1250 °C/ 1h	75	0.3–1.5	
S3-1	1300 °C/ 1h	91	0.6–2.5	
S4-1	1350 °C/ 1h	93	12–33	
S5-1	1400 °C/ 1h	95	15–36	
S6-1	1450 °C/ 1h	95	30–85	
S1-10	1200 °C/ 10h	69	0.5–1.7	
S2-10	1250 °C/ 10h	90	0.8–3	
S3-10	1300 °C/ 10h	95	2–7	
S4-10	1350 °C/ 10h	97	16–70	
S5-10	1400 °C/ 10h	98	22–94	
S6-10	1450 °C/ 10h	98	24–100	

1) calculated from the specific surface area

2) volume-weighted average crystallite size (Scherrer equation)

3) prepared from powder **1a**, the relative density is in relation to 6.64 g/cm³

4) determined from SEM images

Table 2

Maximal magnetization (M_{max})¹⁾, coercivity (H_c) and remanence (M_r) of synthesized LaFeO₃ powders and ceramics at 300 K and 10 K

Sample	300 K			10 K			
	M _{max} (emu/g) ¹⁾	H _c (kOe)	M _r (emu/g)	M _{max} (emu/g) ¹⁾	H _c (kOe) ²⁾	ΔH _c (kOe) ³⁾	M _r (emu/g)
powder 1a	1.05	19.5	0.23	1.36	14.4	7.0	0.27
powder 1b	1.03	23.8	0.21	1.03	25.9	12.3	0.25
powder 1c	0.86	28.3	0.20	1.01	27.1	7.0	0.23
powder 1d	0.90	31.7	0.23	0.99	36.3	5.6	0.27
powder 1e	0.85	29.6	0.20	0.92	34.4	4.4	0.24

ceramic S1-1	0.90	32.8	0.25	1.00	37.7	0.29
ceramic S2-1	1.02	32.1	0.35	1.14	36.3	0.42
ceramic S3-1	1.19	13.7	0.46	1.31	14.1	0.53
ceramic S4-1	1.21	5.7	0.48	1.33	5.8	0.55
ceramic S5-1	1.20	5.1	0.48	1.34	5.2	0.55
ceramic S6-1	1.20	4.3	0.49	1.36	4.4	0.56
ceramic S1-10	0.97	35.1	0.32	1.09	39.3	0.39
ceramic S2-10	1.11	21.3	0.43	1.31	14.1	0.53
ceramic S3-10	1.21	8.0	0.46	1.34	7.9	0.53
ceramic S4-10	1.21	3.7	0.50	1.34	3.7	0.56
ceramic S5-10	1.16	3.5	0.48	1.29	3.6	0.55
ceramic S6-10	1.15	3.0	0.47	1.27	3.0	0.54

¹⁾ magnetization at 90 kOe

²⁾ collected at negative field (absolute value)

³⁾ calculated from $\Delta H_c = |0.5(H_{c(df)} + H_{c(if)})|$

Table 3

Optical band gaps of LaFeO₃ powders and ceramics

Sample	E _g (eV)
powder 1a	2.65(2)
powder 1b	2.64(2)
powder 1c	2.66(2)
powder 1d	2.67(1)
powder 1e	2.64(3)
ceramic S1-1	2.51(4)
ceramic S3-1	2.13(1)
ceramic S6-1	2.12(1)
ceramic S1-10	2.48(2)
ceramic S3-10	2.17(2)
ceramic S6-10	2.16(2)

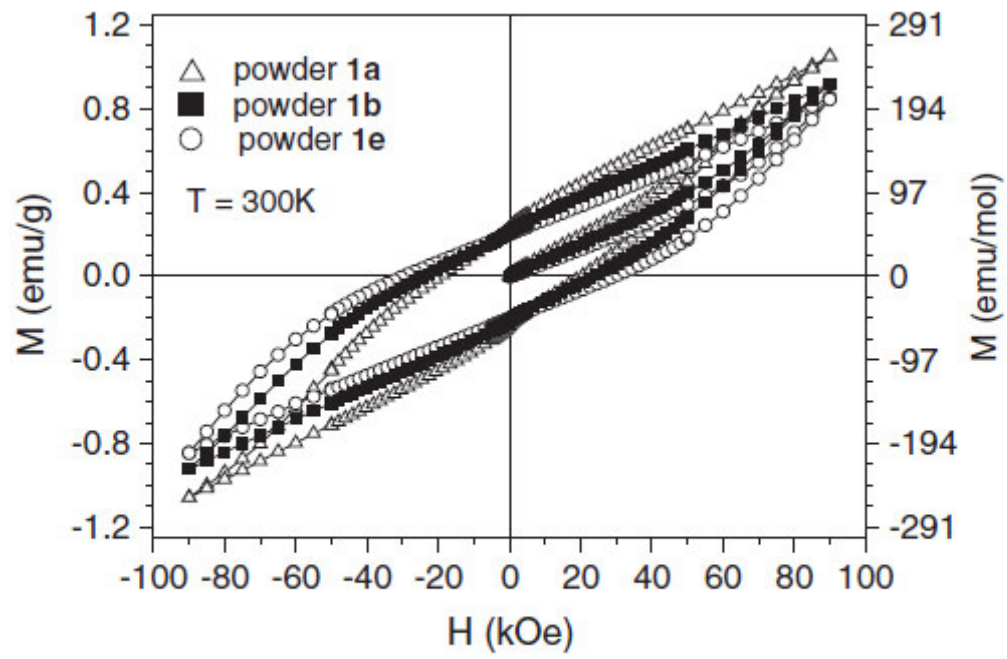


Fig. 1. M-H hysteresis loops at 300 K of LaFeO_3 powders 1a, 1b, and 1e.

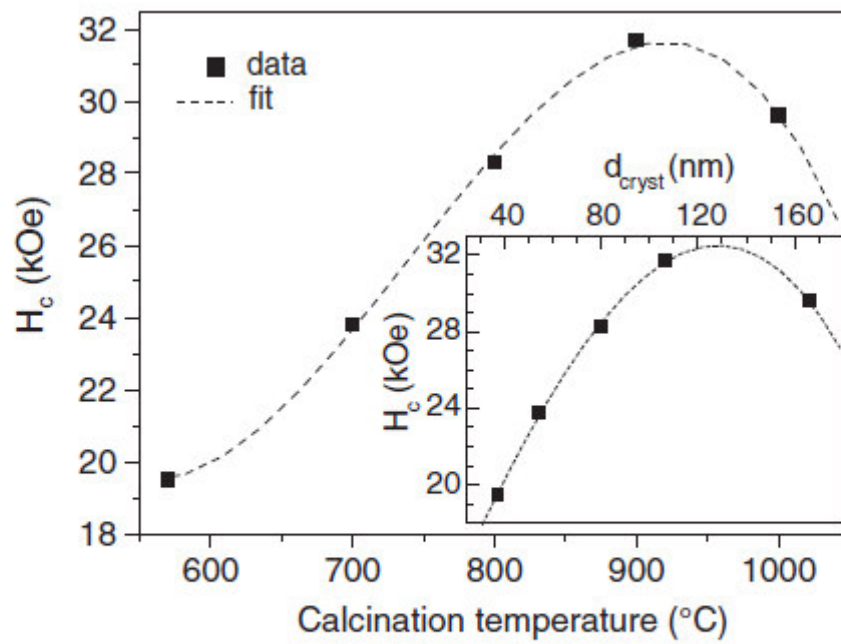


Fig. 2. Dependence of coercivity (H_c) on calcination temperature and crystallite size (inset) at 300 K.

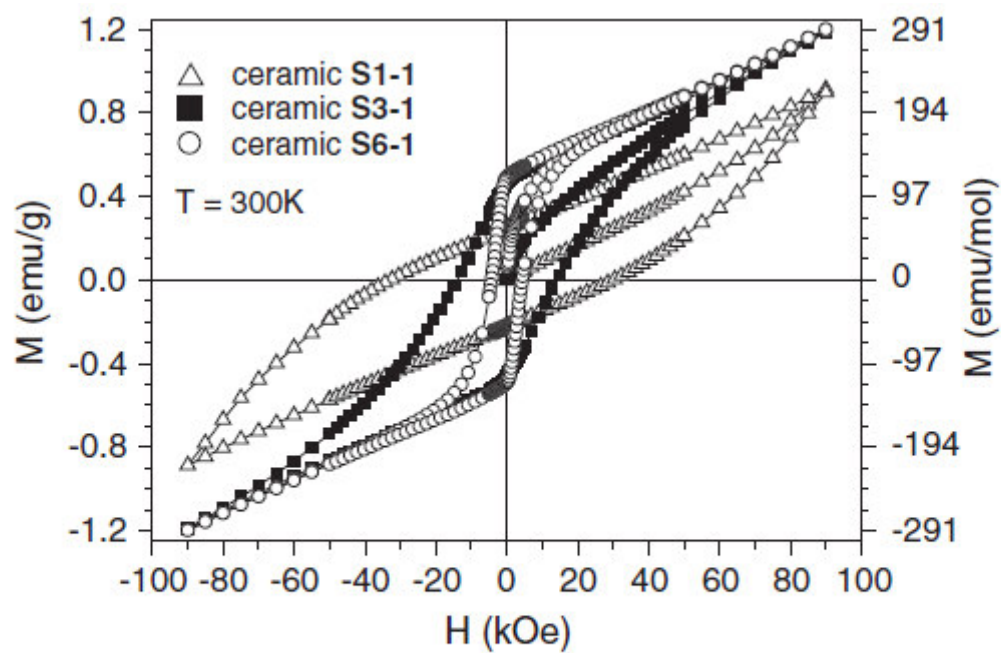


Fig. 3. M-H hysteresis loops at 300 K of LaFeO₃ ceramics made from powder 1a sintered for 1 h at 1200 °C (S1-1), 1300 °C (S3-1), and 1450 °C (S6-1).

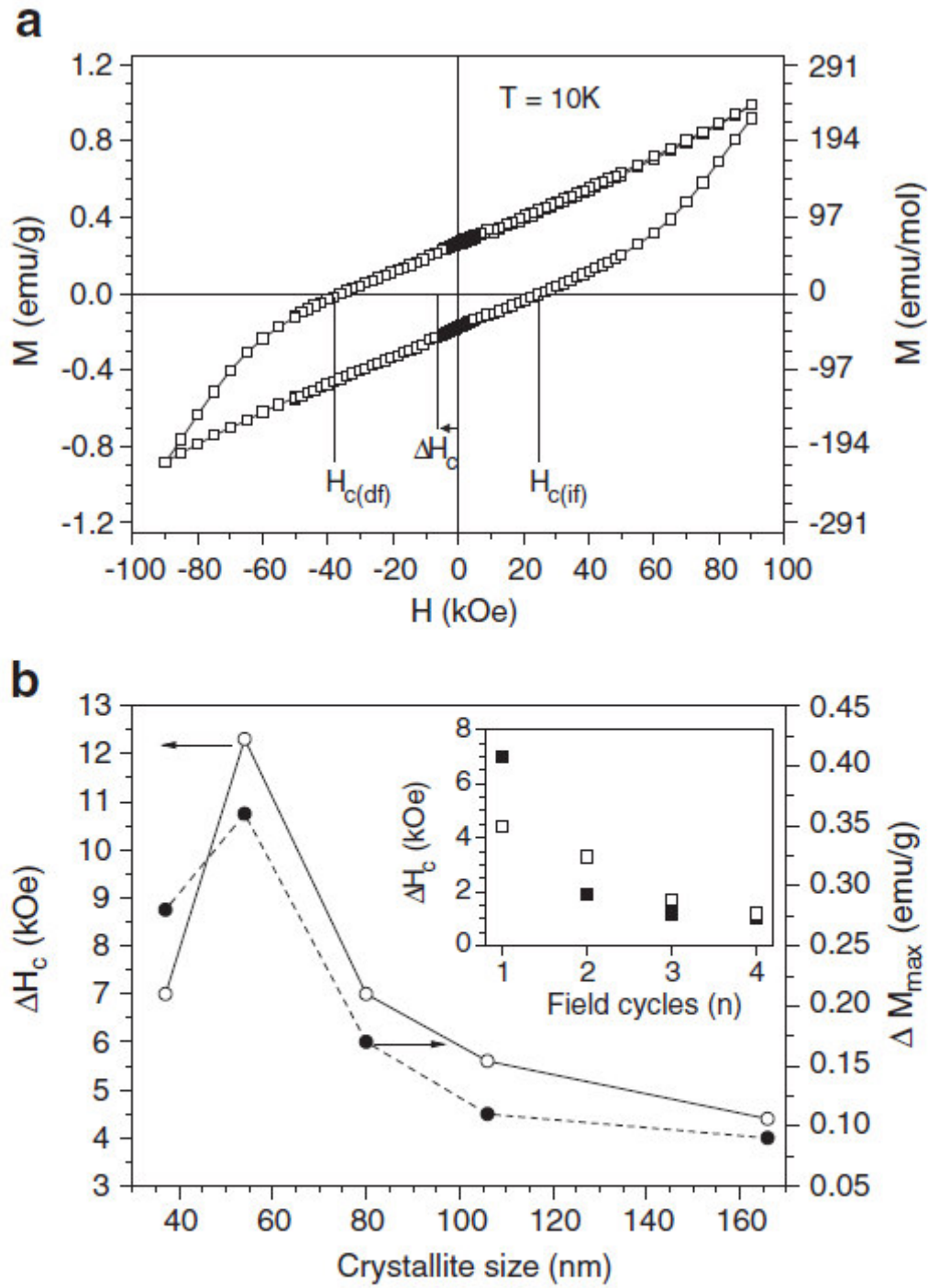


Fig. 4. (a) M–H hysteresis loop of powder 1d at 10 K. The coercivity shift (ΔH_c), the coercivity at decreasing field ($H_{c(df)}$) and increasing field ($H_{c(if)}$) are indicated in the figure. (b) Shift of the coercivity (ΔH_c) and difference of the maximum magnetization (ΔM_{max}) at $H = \pm 90$ kOe versus crystallite size (powders 1a–1e). The inset shows the dependence of ΔH_c on the number (n) of consecutive hysteresis loops for powders 1a (■) and 1e (□), respectively.

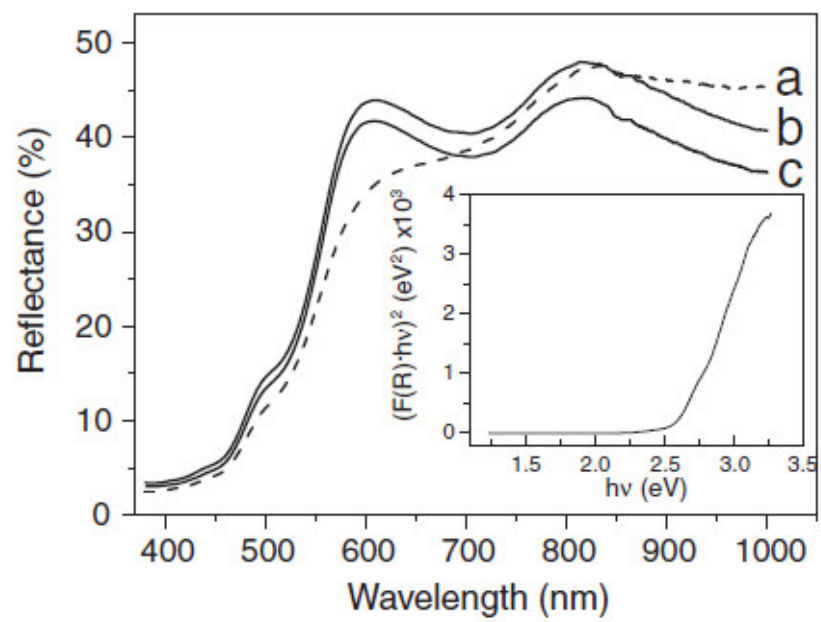


Fig. 5. Diffuse reflectance spectra of powders 1a (a), 1c (b), and 1e (c). The inset shows $(F(R) \cdot h\nu)^2$ vs. $h\nu$ of powder 1a.

References

- [1] E.V. Tsipis, M.V. Patrakeeve, V.V. Kharton, A.A. Yaremchenko, G.C. Mather, A.L. Shaula, I.A. Leonidov, V.L. Kozhevnikov, J.R. Frade, *Solid State Sci.* 7 (2005) 355–365.
- [2] C.-Y. Tsai, A.G. Dixon, W.R. Moser, Y.H. Ma, *AIChE J.* 43 (1997) 2741–2750.
- [3] J. Deng, H. Dai, H. Jiang, L. Zhang, G. Wang, H. He, C.T. Au, *Environ. Sci. Technol.* 44 (2010) 2618–2623.
- [4] Y.-G. Cho, K.-H. Choi, Y.-R. Kim, J.-S. Jung, S.-H. Lee, *Bull. Korean Chem. Soc.* 30 (2009) 1368–1372.
- [5] A.E. Giannakas, A.K. Ladavos, P.J. Pomonis, *Appl. Catal. B-Environ.* 49 (2004) 147–158.
- [6] A.A. Barresi, D. Mazza, S. Ronchetti, R. Spinicci, M. Vallino, *Stud. Surf. Sci. Catal.* 130 (2000) 1223–1228.
- [7] F. Magalhães, F.C.C. Moura, J.D. Ardisson, R.M. Lago, *Mater. Res.* 11 (2008) 307–312.
- [8] J. Faye, E. Guelou, J. Barrault, J.M. Tatibouet, S. Valange, *Top. Catal.* 52 (2009) 1211–1219.
- [9] K.M. Parida, K.H. Reddy, S. Martha, D.P. Das, N. Biswal, *Int. J. Hydrogen. Energ.* 35 (2010) 12161–12168.
- [10] P. Tang, M. Fu, H. Chen, F. Cao, *Mater. Sci. Forum* 694 (2011) 150–154.
- [11] Y. Wang, X. Yang, L. Lu, X. Wang, *Thermochim. Acta* 443 (2006) 225–230.
- [12] P. Song, H. Quin, L. Zhang, K. An, Z. Lin, J. Hu, M. Jiang, *Sens. Actuators B* 104 (2005) 312–316.
- [13] E.N. Armstrong, T. Striker, V. Ramaswamy, J.A. Ruud, E.D. Wachsman, *Sens. Actuators B* 158 (2011) 159–170.

-
- [14] P. Song, Q. Wang, Z. Zhang, Z. Yang, *Sens. Actuators B* 147 (2010) 248–254.
- [15] K. Huang, H.Y. Lee, J.B. Goodenough, *J. Electrochem. Soc.* 145 (1998) 3220–3227.
- [16] T.H. Shin, S. Ida, T. Ishihara, *J. Am. Chem. Soc.* 133 (2011) 19399–19407.
- [17] M.-H. Hung, M.V.M. Rao, D.-S. Tsai, *Mater. Chem. Phys.* 101 (2007) 297–302.
- [18] F. Bidrawn, S. Lee, J.M. Vohs, R.J. Gorte, *J. Electrochem. Soc.* 155 (2008) B660–B665.
- [19] J.W. Seo, E.E. Fullerton, F. Nolting, A. Scholl, J. Fompeyrine, J.-P. Locquet, *J. Phys. Condens. Matter* 20 (2008) 264014.
- [20] E. Traversa, P. Nunziante, M. Sakamoto, Y. Sadaoka, M.C. Carotta, G. Martinelli, *J. Mater. Res.* 13 (1998) 1335–1344.
- [21] G. Shabbir, A.H. Qureshi, K. Saeed, *Mater. Lett.* 60 (2006) 3706–3709.
- [22] H. Xu, X. Hu, L. Zhang, *Cryst. Growth Des.* 8 (2008) 2061–2065.
- [23] X. Li, H. Zhang, M. Zhao, S. Li, B. Xu, *J. Mater. Chem.* 2 (1992) 253–254.
- [24] S. Li, L. Jing, W. Fu, L. Yang, B. Xin, H. Fu, *Mater. Res. Bull.* 42 (2007) 203–212.
- [25] M.B. Bellakki, B.J. Kelly, V. Manivannan, *J. Alloys Compd.* 489 (2010) 64–71.
- [26] T. Liu, Y. Xu, *Mater. Chem. Phys.* 129 (2011) 1047–1050.
- [27] F.-T Li, Y. Liu, R.-H. Liu, Z.-M. Sun, D.-S. Zhao, C.-G. Kou, *Mater. Lett.* 64 (2010) 223–225.
- [28] T. Arima and Y. Tokura, *Phys. Rev. B* 48 (1993) 17006–17009.
- [29] M. Sorescu, T. Xu, J.D. Burnett, J.A. Aitken, *J. Mater. Sci.* 46 (2011) 6709–6717.
- [30] M. Popa, J.M. Calderon Moreno, *J. Alloys Compd.* 509 (2011) 4108–4116.
- [31] J. Chandradass, Ki Hyeon Kim, *Mater. Chem. Phys.* 122 (2010) 329–332.
- [32] S.N. Sahu, K.K.Nanda, *PINSA A* 67 (2001) 103–130.
- [33] E. Roduner, *Chem. Soc. Rev.* 35 (2006) 583–592.

-
- [34] I. R. Shein, K. I. Shein, V. L. Kozhevnikov, A. L. Ivanovski, *Phys. Solid State* 47 (2005) 2082–2088
- [35] Z. Yang, Z. Huang, L. Ye, X. Xie, *Phys. Rev. B* 60 (1999) 15674–15682.
- [36] R. Köferstein and S.G. Ebbinghaus, *Solid State Ionics* 231 (2013) 43–48.
- [37] G.O. Müller, Quantitativ-anorganisches Praktikum, 7th ed., Harry Deutsch, Frankfurt/Main, 1992.
- [38] E.-G. Jäger, K. Schöne, G. Werner, Elektrolytgleichgewichte und Elektrochemie (Arbeitsbuch 5), 4th ed. VEB Deutscher Verlag für Grundstoffindustrie, Leipzig, 1989.
- [39] V.D. Allred, S.R. Buxton, J.P. McBride, *J. Phys. Chem.* 61 (1957) 117–120.
- [40] J. Nogues and I.K. Schuller, *J. Magn. Magn. Mater.* 192 (1999) 203–232.
- [41] D.L. Leslie-Pelecky and R.L. Schalek, *Phys. Rev. B* 59 (1999) 457–462.
- [42] R.H. Kodama, S.A. Makhlof, A.E. Berkowitz, *Phys. Rev. Lett.* 79 (1997) 1393–1396.
- [43] R. Maiti, S. Basu, D. Chakravorty, *J. Magn. Magn. Mater.* 321 (2009) 3274–3277.
- [44] L. Wu, C. Dong, H. Chen, J. Yao, C. Jiang, D. Xue, *J. Am. Ceram. Soc.* 95 (2012) 3922–3927.
- [45] Z.M. Tian, S.L. Yuan, X.L. Wang, X.F. Zheng, S.Y. Yin, C.H. Wang, L. Liu, *J. Appl. Phys.* 106 (2009) 103912.
- [46] D. Wang and M. Gong, *J. Appl. Phys.* 109 (2011) 114304.
- [47] H. Ahmadvand, H. Salamati, P. Kameli, A. Poddar, M. Acet, K. Zakeri, *J. Phys. D: Appl. Phys.* 43 (2010) 245002.
- [48] D. Paccard, C. Schlenker, O. Massenet, R. Montmory, A. Yelon, *phys. stat. sol.* 16 (1966) 301–311.
- [49] C. Schlenker, S.S.P. Parkin, J.C. Scott, K. Howard, *J. Magn. Magn. Mater.* 54–57 (1986) 801–802.

-
- [50] Z.M. Tian, S.L. Yuan, L. Liu, S.Y. Yin, L.C. Jia, P. Li, S.X. Huo, J. Q. Li, *J. Phys. D: Appl. Phys.* 42 (2009) 035008.
- [51] Q. K. Ong, X.-M. Lin, A. Wei, *J. Phys. Chem. C* 115 (2011) 2665–2672.
- [52] P. K. Manna, S.M. Yusuf, R. Shukla, A.K. Tyagi, *Phys. Rev. B* 83 (2011) 184412.
- [53] E.C. Passamani, B.R. Segatto, C. Larica, R. Cohen, J.M. Greneche, *J. Magn. Magn. Mater.* 322 (2010) 3917–3925.
- [54] J. Nogues, J. Sort, V. Langlais, V. Skumryev, S. Surinach, J.S. Munoz, M.D. Baro, *Phys. Rep.* 422 (2005) 65–117.
- [55] H. Shen, G. Cheng, A. Wu, J. Xu, J. Zhao, *Phys. Status Solidi A* 206 (2009) 1420–1424.
- [56] N.T. Thuy and D.L. Minh, *Adv. Mater. Sci. Eng.* (2012) 380306.
- [57] S. Chikazumi, *Physics of Ferromagnetism*, second ed., Oxford University Press Inc., New York, 1997, pp.151.
- [58] M.B. Bellakki, V. Manivannan, C. Madhu, A. Sundaresan, *Mater. Chem. Phys.* 116 (2009) 599–602.
- [59] P. Kubelka and F. Munk, *Z. Techn. Phys.* 11 (1931) 593–601.
- [60] G. Kortüm and J. Vogel, *Z. Phys. Chem.* 18 (1958) 110–122.
- [61] M. Nowak, B. Kauch, P. Szperlich, *Rev. Sci. Instrum.* 80 (2009) 046107.
- [62] R. Lopez and R. Gomez, *J. Sol-Gel Sci. Technol.* 61 (2012) 1–7.
- [63] S. Thirumalairajan, K. Giriya, I. Ganesh, D. Mangalaraj, C. Viswanathan, A. Balamurugan, N. Ponpandian, *Chem. Eng. J.* 209 (2012) 420–428.
- [64] R. Köferstein, F. Yakuphanoglu, *J. Alloys Compd.* 506 (2010) 678–682.
- [65] T.P McLean, in: A.F. Gibson (Ed.), *Progress in Semiconductors*, Vol. 5, 1960, pp. 55–102.
- [66] O. Schevciw and W. B. White, *Mater. Res. Bull.* 18 (1983) 1059–1068.
- [67] S.M. Sze, *Physics of Semiconductor Devices*, J. Wiley & Sons, 1969, p. 52.